



Contents lists available at ScienceDirect

Energy

journal homepage: www.elsevier.com/locate/energy

Distributed real-time power management for virtual energy storage systems using dynamic price

Wenfa Kang^{*}, Minyou Chen^{**}, Wei Lai, Yanyu Luo

State Key Laboratory of Power Transmission Equipment & System Security and New Technology, School of Electrical Engineering, Chongqing University, Chongqing, 400044, China

ARTICLE INFO

Article history:

Received 20 May 2020

Received in revised form

6 October 2020

Accepted 11 October 2020

Available online xxx

Keywords:

Virtual energy storage system

Dynamic pricing strategy

Distributed optimization

Time-varying directed network

Power management

ABSTRACT

Energy storage systems (ESS) are widely used in active distribution networks (ADN) to smoothen the drastic fluctuation of renewable energy sources (RES). In order to enhance the scalability and flexibility of ESS, a virtual energy storage system (VESS), which is composed of battery energy storage system (BESS), RES as well as flexible loads (FL), is developed in this paper to realize the functionalities of ESS in more cost-effective way in ADN. Aiming at achieving voltage regulation, dynamic pricing strategies based on system voltage condition are designed for VESS. A distributed real-time power management model containing dynamic pricing strategies is proposed to accomplish the voltage regulation and economic power sharing in VESS. Moreover, a set of distributed algorithms, over time-varying unbalanced directed networks, are designed for dynamic pricing strategies and optimal power management model. Furthermore, the convergence property, optimality and system voltage stability are explained by detailed mathematical analysis. Three various case studies which were ran on a real time digital simulator (OPAL-RT OP5600) were designed to validate the effectiveness of the strategy. Finally, simulation results show that the economic power dispatch and voltage regulation are achieved among VESS simultaneously, even in the presence of time-varying directed and unbalanced communication networks.

© 2020 Elsevier Ltd. All rights reserved.

1. Introduction

1.1. Motivation

The active distribution network (ADN), a meritorious technical means to realize the wide access of renewable energy sources (RES), plays pivotal role in power system. Usually, wind turbines (WT), photovoltaic sources (PV), are within the conception of RES. RES with high randomness, intermittence and fluctuation widely adopts power electronic devices to integrate into the ADN, which has brought huge challenges to the dynamic balance of power supply and demand, safety, and stability of grid [1]. Promisingly, technologies, such as advanced converter control methods, power and energy management strategies, demand response, optimal power flow schemes and energy trading frameworks, are utilized to address these challenges to accomplish the comprehensive and

efficiency utilization of diverse resources [2,3]. To the discussion of RES integration, microgrids (MG) with RES, BESS, distributed generators (DG) and maybe flexible loads (FL) are popular research fields to harvest clean and green energy [4,5]. Inevitably, power congestion caused by stochastic, intermittent outputs of RES and fluctuated load demand will lead to system power imbalance, low/high frequency and voltage variation, which in turn results in energy waste or even system stability issue of MG [6,7]. Although oil or gas-burning generators, like diesel generators and micro turbines, are employed in MG to guarantee system power supply-demand balance, frequency and voltage stability, air and noise pollution caused by their operation are still a pending issue. Fortunately, BESS, which are widely used in power system to smoothen fluctuation of RES and load demand, provide voltage and frequency support for MG, are promising alternatives of gas-burning generators. Besides, continuously decreasing cost and rapid response facilitate various applications of BESS in MG and ADN, such as frequency control, voltage regulation as well as peaking shaving [8–10].

^{*} Corresponding author.

^{**} Corresponding author.

E-mail addresses: kwf.ac@outlook.com (W. Kang), minyouchen@cqu.edu.cn (M. Chen).

List of abbreviations**Parameters**

$\alpha_i, \beta_i, \gamma_i$	Economic parameters of BESS Active Power
ΔT	Battery charging/discharging period
η_i, v_i	Economic parameters of FL active Power
ω	Power factor
ξ_i	Battery charging/discharging efficiency
A	The reduced branch-bus incidence matrix
a_{Bi}, b_{Bi}	Economic parameters of BESS of Reactive Power
a_{Fi}, b_{Fi}	Economic parameters of FL reactive Power
a_i, b_i	Economic parameters of PV active Power
a_{Vi}, b_{Vi}	Economic parameters of PV Reactive Power
$D(t)$	The out-degree vector
$H(t)$	The weight matrix
I	Identity matrix
$k_p, k_i, C_{penalty}$	Positive constants
$N, \lambda(t), A(t)$	N is the number of nodes, $\lambda(t)$ is the links in the network, $A(t)$ is the adjacent matrix
N_B	Number of BESS
N_L	Number of FL
N_V	Number of PV
P_{Vi}^f	Forecasting power of PV_i
R', X'	Resistance matrix, Reactance matrix
U^{up}, U^{lw}	Upper and lower voltage limit
U_0	System rated voltage

Variables and Functions

Δf_i	Gradient of the objective function
--------------	------------------------------------

$\mu_i(t)$	Dynamic price of node i
$CB_i(t), QB_i(t)$	Active and reactive power cost function of BESS
$CF_i(t), QF_i(t)$	Active and reactive power cost function of FL
$CG_i(t), QG_i(t)$	Active and reactive power cost function of PCC
$CV_i(t), QV_i(t)$	Active and reactive power cost function of PV
$Ld_i(t)$	Local load demand of unit i
$m_i(t), \zeta_i(t)$	Primal and dual variables
$P_{Bi}(t), Q_{Bi}(t)$	Active and reactive power of BESS
$P_G(t), Q_G(t)$	Active and reactive power of PCC
$P_{Li}(t), Q_{Li}(t)$	Active and reactive power of FL
$P_{Vi}(t), Q_{Vi}(t)$	Active and reactive power of PV
$U_i^m(t), U_i^{ave}(t)$	Measured voltage amplitudes, System average voltage amplitude
$V(t)$	Auxiliary variable Vector
$x_i(t), z_i(t), g_i(t)$	Auxiliary variables
$Y(t)$	Weight Vector

Abbreviations

ADN	Active Distribution Network
BESS	Battery Energy Storage System
DG	Distributed Generators
FL	Flexible Load
MBESS	Multiple Battery Energy Storage System
MG	Microgrids
PCC	Point of Common Coupling
PV	photovoltaic source
RES	Renewable Energy Sources
SoC	State of Charge
VESS	Virtual Energy Storage System

1.2. Related work

Growing number of documents pay attention to the energy management, optimal control of BESS and multiple battery energy storage systems (MBESS) [11–16]. Traditionally, centralized methods were proposed to achieve the energy management of BESS and FL [11], demand response [13], power sharing [14,15], frequency control [16] and secondary market service [12]. These methods work in centralized manner, which usually are threatened by the single point failure. However, less attention was paid on the potential of RES to participate these various targets. In Ref. [12], different scenarios of battery participating secondary market service were investigated, where obsolescent EV batteries were aggregated in a building as a battery station to provide frequency services for European power grid. While in Ref. [13], model predictive control method was proposed for BESS and heating system in low voltage distribution networks to join in demand response procedure as well as to reach an economical operation condition. In Ref. [14,15], centralized optimization strategies were adopted for MBESS to improve system efficiency as well as to prolong battery lifetime. A hierarchical MBESS model for power system frequency control was proposed in Ref. [16], where the first layer was to generate control command signals according to the states of charge (SoC) of BESS, while the controllers of second BESS layer were activated according to the command signals to inject/absorb power to/from power grid. As to virtual energy storage system (VESS), Cheng et al. investigated the benefits of VESS on frequency response [17], where VESS was composed of various traditional energy storage systems (electrochemical, mechanical, electrical and thermal energy storage system) and domestic flexible loads which had ability to participate in demand response. While in Ref. [18],

based on thermal storage capacity, air conditioners were modeled as VESS to track regulation signal despite of thermodynamic characteristics and ramping rate limits. In Ref. [19], energy management strategy was proposed for VESS which contained actual batteries and electrical springs to acquire benefits of consumers and utility operators. Besides, the economic dispatch model of MG with batteries and VESS, which was derived from the heat storage capability of the building, was proposed in Ref. [20] to reduce the daily operation cost of system. Furthermore, shipboard thermal storage and thermal load as VESS was adopted in voyage scheduling and power dispatching model to reduce both operating cost and greenhouse gas emissions of all-electric ships [21]. An energy management scheme for residential energy systems was proposed in Ref. [22], where air compressed energy storage system, small PV power plant were the main equipment of the system to fulfill the trigeneration (production of heating, cooling and electricity). In Ref. [23], a decentralized ESS power and bus voltage control for DC MG was proposed, where the ESS branch is equivalent to the virtual-battery model under droop control. A bi-level robust power optimization model for VPP was designed in Ref. [24] to dispatch PV, WT, ESS and FL power in order to maximize VPP income and minimize system cost. Besides, the risk-averse stochastic optimization model considering joint energy and reserve trading for VPP is proposed in Ref. [25], where objective of the proposed model is to maximize the VPP profit and to optimize trading power with the main grid for the purpose of ensuring VPP power quality and satisfying N-1 security. To conclude, virtual energy storage systems (VESS), as augmented energy storage systems (ESS), is studied by several documents in the aspect of ancillary services [18], economic dispatch [20,21], energy management [19] and frequency response [17]. However, the definitions of VESS are various, such as the

model with various traditional ESS (electrochemical, mechanical, electrical and thermal energy storage system) and flexible loads [17], the model which is only composed of air conditioning loads [18], the model with BESS and electrical springs [19], the model with batteries and thermal storage of buildings [20], and model with thermal storage and thermal load [21]. Different from the VESS models discussed above, the model of VESS proposed in this paper contains not only ESS, flexible loads but also RES. The power generation equipment, such as PV, WT, and power consuming devices, like FL and InFL, have potential to provide energy or absorb energy when necessary. Here, the provided and absorbed energy of such kind of equipment are the generalized notion, since FL and InFL can't produce energy no matter how their demands change. However, FL can be regulated to consume less energy when system energy is in shortage, which means FL is capable to provide energy. RES (PV, WT) might curtail its power when system power supply is higher than power demand, so the curtailed energy means that RES can absorb energy from grid. From the points discussed above, such equipment have the similar characteristics with ESS when considering energy providing and absorbing purpose. Moreover, when a lot of the equipment (units) in a certain geographical area connected to the grid, the equipment coordinating together have promising potential to provide or absorb energy to/from grid to participate various applications such as power balancing, peak shaving, energy management as well as ancillary services. Thus we define a system which has potential to provide or absorb energy, acting like ESS, as virtual energy storage system.

Different from MG and VPP, a Virtual Energy Storage System (VESS) is regarded as an aggregation of various controllable components of energy systems, which could include conventional energy storage systems, flexible loads and distributed generators. VESS is a cost-effective way to provide the function of conventional Energy Storage System (ESS) through the utilization of the present network assets represented by the flexible demand. VESS can be treated as an entity in MG or distribution network, acting as ESS to participate energy management, power sharing, voltage and frequency regulation, ancillary services. In this paper the VESS is modeled to store and release energy in response to voltage regulation and economic power sharing by coordinating the demand response (DR) from flexible loads and distributed energy storage systems. The VESS is developed to enhance the functionalities of ESS in more economical way and provide optimal power dispatch strategy for distribution network.

1.3. Main contributions

To generalize documents discussed above, centralized method is indispensable to give command signals to BESS, MBESS or VESS in order to finish their pre-set targets, meanwhile high-speed communication system and rapid central computer are needed in their frameworks. However, distributed strategies, which is different from centralized method, gained popularity [26,27] among the management of MG and ADN, due to the low-communication cost, flexibility, scalability and the potential to avoid single point failure. A decentralized power control method was proposed in Ref. [28] for DC microgrid, where the controller of power sources was based on droop coefficients. MAS based distributed energy management scheme was proposed in Ref. [29] to achieve system power balance and costs minimization, however, the proposed particle swarm optimization algorithm for solving the power dispatch problem was not fully distributed. For multiple MG power sharing, Li et al. proposed MAS based distributed power sharing method [30], where algorithms with dynamic weights was used to dispatch MG power according to MG capacities. However, the proposed algorithm was applied over the undirected time-

invariant and balanced communication networks. Furthermore, ADMM was used in Ref. [31] to dispatch power between multiple MGs and DN economically, meanwhile a centralized coordinator for ADMM optimization algorithm was necessary. Compared with these distributed methods in Ref. [28–31], the proposed methods in this paper is fully distributed, and can be applied over the time-varying unbalanced directed networks. Moreover, the proposed VESS power management scheme can minimize system operation costs and voltage regulation simultaneously.

Therefore, in this paper, distributed optimization model of VESS is proposed to minimize system costs and to keep system voltages in an acceptable range. The model of VESS in this paper not only contains BESS and FL but also RES (PV), since RES connected to distribution network can be regarded as partially controllable power sources. Moreover, the conception of VESS is an augmented version compared with the ideas in Ref. [17–21], since in this paper, from the point of energy consumption and production, the combination of RES and FL could be the units of VESS.

To conclude, the contribution in this paper contains the following four aspects.

- Compared to the model in Ref. [17–21], an augmented version of VESS is proposed, which not only contains BESS and FL but also RES.
- The distributed optimization model and algorithms for VESS are designed, where the distributed algorithms, which can be adapted to the time-varying directed communication network, are capable to solve convex function with equality and inequality constraints.
- The distributed dynamic pricing strategy, which is defined on the system voltage variation, is designed for each unit in VESS. In this way, economical power dispatch and system voltage regulation can be accomplished simultaneously.
- The performance of the proposed method is analyzed, where the convergence and optimality property of the proposed distributed algorithms and pricing strategy are guaranteed by elaborate mathematical analysis.

This paper is organized as follows. In Section II, problem formulation and dynamic pricing strategy for VESS, which is derived from system voltage fluctuation, are proposed. Distributed algorithms for VESS are designed in Section III. While in Section IV, system performance of VESS is analyzed. Real time simulation results and analysis are presented in Section V. Finally, Section VI concludes the paper.

2. System model and problem formulation

In this section, the model of VESS and dynamic pricing rule are described, respectively. VESS model is an economic power dispatching problem (EDP) considering system voltage fluctuation, in other word, the cost functions of BESS, PV and FL depend on not only its inherent economic parameters but also system operation index, i.e., voltage amplitudes. In this way, BESS, PV and FL power are dispatched among system in terms of their costs and local voltage fluctuation. In order to include system voltage into the economic power dispatching problem, the dynamic pricing rule is designed for each unit in VESS according to the local voltage fluctuation.

2.1. Power dispatching model of VESS considering dynamic price

In order to take the battery state of charge (SoC) into the cost function, following quadratic function is adopted for battery energy storage system [32],

$$CB_i(t) = (\alpha_i(P_{Bi}(t) + s_i \cdot (1 - SoC(t))))^2 + (\beta_i - \mu_i(t)) \times (P_{Bi}(t) + s_i \cdot (1 - SoC(t))) + \gamma_i, \quad (1)$$

where $\alpha_i, \beta_i, \gamma_i > 0$, ($i = 1, \dots, N_B$) present running cost, maintenance cost and investment cost (economic parameters), while s_i is the constant and $SoC(t)$ is the state of charge of BESS. While the cost function for reactive power of BESS is,

$$QB_i(t) = a_{Bi}Q_{Bi}(t)^2 - (\mu_i(t) + b_{Bi})Q_{Bi}(t), \quad (2)$$

where a_{Bi} ($i = 1, \dots, N_B$) is the reactive power economic parameter, while $\mu_i(t)$, ($i = 1, \dots, N_B$) is the dynamic price of BESS, which is depend on the system performance.

In distribution network, RES such as PV sources usually work in MPPT mode for the purpose of enhancing the RES penetration. However, this is not an efficient and effective way to harvest clear energy since voltage limits violation issues caused by RES power injection often damage electrical equipment [2,33]. In this paper, PV sources are assumed to be adjustable with the help of the short time power forecasting technique [34]. Coherently, the PV power management method, such as PV power curtailment method proposed in Ref. [35], usually provide positive effects on system voltage regulation. Therefore, in the paper, in order to minimize the amount of curtailed real power, the cost function of PV active power is formulated as,

$$CV_i(t) = a_i(P_{Vi}(t) - P_{Vi}^f)^2 + (b_i - \mu_i(t))(P_{Vi}(t) - P_{Vi}^f), \quad (3)$$

where $a_i > 0$, $b_i > 0$, ($i = 1, \dots, N_V$) are economic parameters, while P_{Vi}^f is the forecasting power of PV. The expression $(P_{Vi}(t) - P_{Vi}^f)$ shows the curtailed PV power. In equation (3), if PV power can not be adjusted, namely, $P_{Vi}(t)$ equals PV, if all the time, the cost of PV sources will be zero, since no PV power curtailment occurs. The quadratic term $a_i(P_{Vi}(t) - P_{Vi}^f)^2$ can be used to express the cost of PV inverters, while the linear term $(b_i - \mu_i(t))(P_{Vi}(t) - P_{Vi}^f)$ could be the wasted cost induced by PV power curtailment. Note that the dynamic price $\mu_i(t)$, associated with system voltage condition, is included in the linear term to adjust PV power according to the system voltage.

Similarly, for PV reactive power cost function proposed in (4),

$$QV_i(t) = a_{Vi}Q_{Vi}(t)^2 - (\mu_i(t) + b_{Vi})Q_{Vi}(t), \quad (4)$$

where a_{Vi}, b_{Vi} , ($i = 1, \dots, N_V$) are the economic parameters and the quadratic term can be understood as a penalization on large reactive power injection in order to provide more flexibility in supplying active power [36,37]. The second term with dynamic price is used to adjust the reactive power according to the system voltage condition.

To evaluate benefit of FL, the quadratic utility function is formulated as,

$$CF_i(t) = -\eta_i P_{Li}(t)^2 + v_i P_{Li}(t), \quad (5)$$

$$QF_i(t) = a_{Fi} Q_{Li}(t)^2 + b_{Fi} Q_{Li}(t),$$

where $\eta_i > 0$, $v_i > 0$ and a_{Fi}, b_{Fi} , ($i = 1, \dots, N_L$) are the economic parameters, while $P_{Li}(t)$ is the load demand of flexible loads i.

For PCC unit, its objective functions are as,

$$CG(t) = P_G(t)^2, \quad (6)$$

$$QG(t) = Q_G(t)^2.$$

To conclude, the operation model of a VESS can be reformulated as following optimization problem,

$$\begin{cases} \text{minimize} \left[\sum_{i=1}^{N_B} CB_i(t) + \sum_{i=1}^{N_V} CV_i(t) + \sum_{i=1}^{N_L} CF_i(t) + CG(t), \right. \\ \left. \sum_{i=1}^{N_B} QB_i(t) + \sum_{i=1}^{N_V} QV_i(t) + \sum_{i=1}^{N_L} QF_i(t) + QG(t) \right], \end{cases} \quad (7)$$

while the corresponding constraints are,

$$\begin{cases} P_{Bmin,i} \leq P_{Bi}(t) \leq P_{Bmax,i}, i \in N_B, \\ P_{Vmin,i} \leq P_{Vi}(t) \leq P_{Vmax,i}, i \in N_V, \\ P_{Lmin,i} \leq P_{Li}(t) \leq P_{Lmax,i}, i \in N_L, \\ P_{Gmin} \leq P_G(t) \leq P_{Gmax}, \\ Q_{Gmin} \leq Q_G(t) \leq Q_{Gmax}, \\ SoC_i(t) = SoC_i(0) - \xi_i \cdot P_{Bi}(t) \cdot \Delta T, \\ SoC_{min} \leq SoC_i(t) \leq SoC_{max}, \\ -\omega P_{Bi}(t) \leq Q_{Bi}(t) \leq \omega P_{Bi}(t), i \in N_B, \\ -\omega P_{Vi}(t) \leq Q_{Vi}(t) \leq \omega P_{Vi}(t), i \in N_V, \\ \sum_{i \in N_V} P_{Vi}(t) + \sum_{i \in N_B} P_{Bi}(t) + \sum_{i \in N_L} P_{Li}(t) \\ + P_G(t) = 0, \end{cases} \quad (8)$$

where $\xi_i, \Delta T$ are the battery charging/discharging efficiency and period, while $\omega = \arccos(\tan(\varphi))$ (φ is the required angle of power factor). $P_G(t), Q_G(t)$ are the active power and reactive power flowing through the PCC point.

Remark 1. The proposed model of VESS (7) and (8) is an economic power dispatching problem with inequality and equality constraints. The power dispatching model (7) contains two parts, the active power and reactive power optimization parts. While the constraints presented in (8) contains power limits constraints, SoC limits constraints and active power balance constraint. Specially, the reactive power limits of BESS and PV are restricted by the power factor and active power. In order to decrease the voltage deviation caused by the penetration of RES, the voltage based dynamic pricing rule is introduced to adjust the power of BESS and PV according to the voltage condition.

2.2. Distributed voltage based pricing rule

In this section, a distributed dynamic pricing strategy for VESS, which is based on the system voltage condition, is provided. In Fig. 1, each controllable unit including PV, BESS and FL regulates its power according to the system power demand-supply balance. Besides, the dynamic price $\mu_i(t)$, representing system voltage performance, is also a vital signal to adjust the outputs/demands of each unit. Hence, each unit regulates its power not only according to the inherent economic parameter but also depending on the system performance index.

System voltages are important factor which imply the system operation condition. While in works [38,39], the information of node voltages is fed back to the PV control models as real-time price signal to adjust the PV active and reactive power in order to diminish voltage deviations. Inspired by the mentioned idea, this paper adopts the voltage information as dynamic price to adjust the active and reactive power of BESS and PV units. The distributed

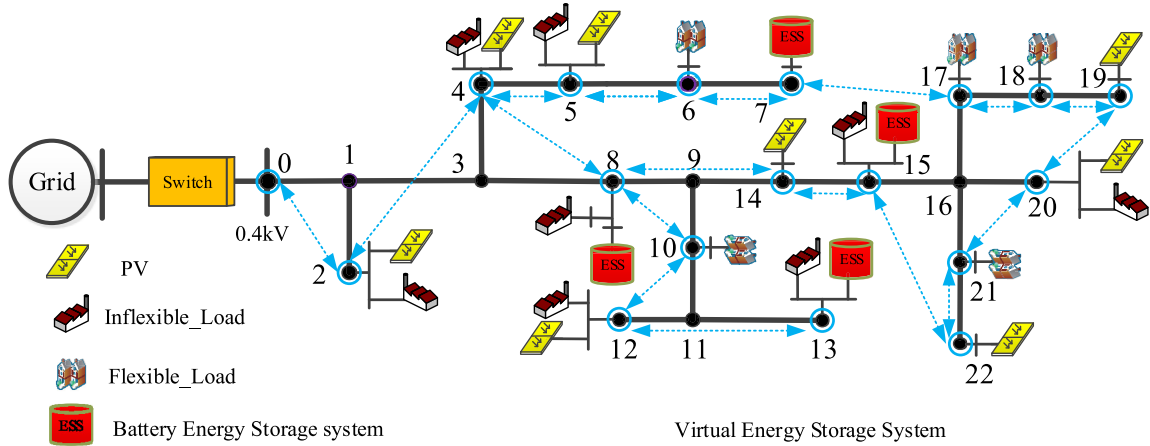


Fig. 1. VESS integrates BESS, PV, FL and inflexible loads, where black line represents power transmission line, blue dash line represents communication link. (For interpretation of the references to colour in this figure legend, the reader is referred to the Web version of this article.)

dynamic price $\mu_i(t)$ which represents the fluctuation of the system voltage, is formulated,

$$\begin{cases} \dot{\rho}_i(t) = k_p \left(\dot{U}_i^{ave}(t) - \dot{U}_i^m(t) \right) + k_i (U_i^{ave}(t) - U_i^m(t)), \\ \mu_i(t) = f_i(\rho_i(t)) \end{cases} \quad (9)$$

where $U_i^{ave}(t)$ represents the system average voltage magnitude estimated by each unit. k_i, k_p are the positive parameters need to be designed. The function $f_i(\rho_i(t))$ is defined as,

$$f_i(\rho_i(t)) = \begin{cases} \rho_i(t) - C_{penalty} (U_i^m(t) - U^{up}), & U_i^m(t) > U^{up}, \\ \rho_i(t), & \\ \rho_i(t) + C_{penalty} (U^{lw} - U_i^m(t)), & U_i^m(t) < U^{lw}, \end{cases} \quad (10)$$

where $C_{penalty}$ is a negative constant while U^{up}, U^{lw} are the system maximum and minimum voltage [39]. If $U_i^m(t) > U^{up}$, its price increases and node i will inject less power, and vice versa. If the voltage limits aren't violated, the price of each unit will stay unchanged. The framework of dynamic pricing strategy for each unit is shown in Fig. 2.

From equations (9) and (10), it can be seen that dynamic price $\mu_i(t)$ is related to the system average voltage and its local voltage. Therefore each unit should have ability to acquire the information of system average voltage in order to get its price. Here, we provide distributed algorithms, which can be applied on the time-varying communication networks, for units in VESS to estimated the

system average voltage, represented as follows.

3. Distributed solutions for VESS

This section designs distributed algorithms for dynamic pricing rule (9) and economic dispatching problem (7) and (8). The proposed algorithms are enable to adapt the time-varying communication networks and directed unbalancing graphs, for which we give a full mathematical analysis.

3.1. Distributed voltage estimation algorithm for dynamic pricing rule

Theorem 1. Assume there is uniformly jointly strongly connected communication network $G(N, \lambda(t), A(t))$, which is time-varying and directed, over the VESS, the system average magnitude $U_i^{ave} = \frac{1}{N} \sum_{i=1}^N U_i(t) |_{t \rightarrow \infty}$ will be estimated by each controllable unit when they conduct the calculation according to the following laws (11),

$$\begin{bmatrix} U^{ave}(t+1) \\ V(t+1) \end{bmatrix} = \begin{bmatrix} I + H(t) & -H(t) \\ -\frac{1}{2}I & I \end{bmatrix}_{2N \times 2N} \begin{bmatrix} U^{ave}(t) \\ V(t) \end{bmatrix}, \quad (11)$$

where matrix I is the identity matrix, while the time-varying weight matrix $H(t) = [h_{ij}(t)]_{N \times N}$ is calculated by the following rules,

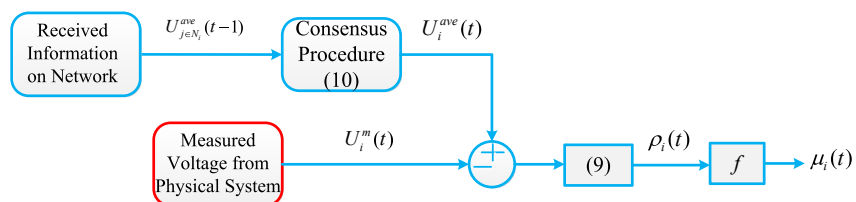


Fig. 2. The framework of dynamic pricing strategy for each unit.

$$H(t) = \begin{bmatrix} -d_1(t)y_1(t) & \cdots & a_{1,j}(t)y_j(t) & \cdots & a_{1,N}(t)y_N(t) \\ \vdots & \ddots & \vdots & \ddots & \vdots \\ a_{j,1}(t)y_1(t) & \cdots & -d_j(t)y_j(t) & \cdots & a_{j,N}(t)y_N(t) \\ \vdots & \ddots & \vdots & \ddots & \vdots \\ a_{N,1}(t)y_1(t) & \cdots & a_{N,j}(t)y_j(t) & \cdots & -d_N(t)y_N(t) \end{bmatrix}, \quad (12)$$

where weight vector $Y(t) = [y_1(t), \dots, y_j(t), \dots, y_N(t)]^T$ is decided by following weight balancing rule,

$$Y(t+1) = \frac{1}{2} (I + D(t)^{-1}A(t))Y(t). \quad (13)$$

Matrix $A(t) = [a_{ij}(t)]_{N \times N}$ is the adjacent matrix of the graph G , while matrix $D(t) = [d_1(t), \dots, d_j(t), \dots, d_N(t)]^T$ is the out-degree vector of nodes.

In expressions (11) and (12), $U^{ave}(t) = [U_1^{ave}(t), \dots, U_N^{ave}(t)]^T$ is the estimated average voltage vector, while $V(t)$ is the auxiliary vector. According to the [Theorem 1](#), each unit will observe the system average voltage via distributed observing laws (11), (12) and (13) in spite of time-varying communication network and changing weights. Each unit only sends and receives three kinds of information, i.e., $U_i^{ave}(t)$, $V_i(t)$ and $y_i(t)$ to and from its neighbors. In other words, only $U_i^{ave}(t)$, $V_i(t)$ and $y_i(t)$ are transmitted over the time-varying network. The weight balancing rule (13), which was first mentioned in [40], guarantees that each unit will have capability to get the average voltage value when converges, i.e., $U_1^{ave}(t) = \dots = U_j^{ave}(t) = \dots = U_N^{ave}(t) = \frac{1}{N} \sum_{i=1}^N U_i(0) |_{t \rightarrow \infty}$.

Proof. See in Appendix.

3.2. Distributed dual-based optimization algorithm over time-varying digraphs

In order to solve the optimal power dispatch problem (7), we instead solve its dual problem regarding to constraints (8) and propose the following distributed optimization algorithm.

Theorem 2. Assume there is a set of time-varying directed communication networks $G(N, \lambda(t), A(t))$ over the VESS, while each node (controllable unit) estimates the information of its power generation and/or load demand from VESS. If the network $G(N, \lambda(t), A(t))$ is uniformly jointly strongly connected, each controllable unit, which shares information over network $G(t)$, will solve the problem (7) with constraints (8) after iterations, according to the following distributed dual-based optimization algorithm,

$$\begin{cases} m_i(t+1) = \operatorname{argmin}_{m \in (m_{i,\min}, m_{i,\max})} \{F_i(m) - \zeta_i(t)(m - Ld_i(t))\}, \\ x_i(t+1) = \varepsilon(t)x_i(t) + (1 - \varepsilon(t))m_i(t+1), \\ z_i(t+1) = \sum_{j \in N_i^m(t) \cup i} h_{ij}(t)z_i(t) - g_i(t), \\ g_i(t+1) = \sum_{j \in N_i^m(t) \cup i} h_{ij}(t)g_i(t) \\ \quad + \varepsilon(t)((x_i(t+1) - Ld_i(t)) - (x_i(t) - Ld_i(t))), \\ \zeta_i(t+1) = \varepsilon(t)\zeta_i(t) + (1 - \varepsilon(t))z_i(t+1), \end{cases} \quad (14)$$

where $Ld_i(t)$ is the load demand of unit i , while $h_{ij}(t)$ is the element of time-varying matrix $H(t)$ defined in [Theorem 1](#). $\varepsilon(t) = \frac{1}{1+t}$ is the tuning parameter. $x_i(t)$, $z_i(t)$, $g_i(t)$ are the auxiliary parameters of optimization algorithm, while $N_i^m(t)$ is the neighbors of unit i .

Moreover, variables $m_i(t)$ and $\zeta_i(t)$ are the primal variables and dual variables respectively.

Proof. See in Appendix.

In order to give explanation about the implementation of the proposed distributed optimization algorithm into the VESS, the optimization process of BESS is taken as an example and explained. The objective function of BESS unit $i \in N_B$:

$$\begin{cases} F_i(t) = [CB_i(t), QB_i(t)], \\ P_{Bmin,i} \leq P_{Bi}(t) \leq P_{Bmax,i}, \\ \frac{SoC(0) - SoC_{max}}{\xi_i \Delta T} \leq P_{Bi}(t) \leq \frac{SoC(0) - SoC_{min}}{\xi_i \Delta T}, \\ -\omega P_{Bi}(t) \leq Q_{Bi}(t) \leq \omega P_{Bi}(t), \\ PB_i(t) = Ld_i(t). \end{cases} \quad (15)$$

Besides, the global equality constraints, such as $\sum_{i \in N_V} PV_i(t) + \sum_{i \in N_B} PB_i(t) + \sum_{i \in N_L} PL_i(t) + PG(t) = 0$, must be satisfied when solving the optimal power dispatch problem (7) using the proposed optimization algorithm. While the global power balance constraint usually can be divided into local constraint according to the power transmission network or communication network by assigning each unit with nearby loads. Assume each uncontrollable load is assigned to each controllable unit (PV, BESS, FL), then power balance constraint is divided into local equality constraints. If local load demand for unit i is $Ld_i(t)$, adopting optimal algorithm (14), the optimization process of unit i is derived as.

Step 0: Initialize $\zeta_i(0) = x_i(0) = z_i(0) = [0, 0]^T$.

Step 1: Solve the following local optimal problem,

$$m_i(t+1) = \operatorname{argmin} \{CB_i(x) + QB_i(y) \quad (16)$$

$$- \zeta_{x,i}(t)(x - Ld_i(t)) - \zeta_{y,i}(t)y\}$$

with constraints,

$$P_{Bi,\min} \leq x_i \leq P_{Bi,\max}, \quad (17)$$

$$\frac{SoC(0) - SoC_{max}}{\xi_i \Delta T} \leq x_i \leq \frac{SoC(0) - SoC_{min}}{\xi_i \Delta T},$$

$$-\omega x_i \leq y_i \leq \omega x_i.$$

Step 2: Get the primal results $m_i(t+1) = [x_i(t+1), y_i(t+1)]^T$ and conduct following expression,

$$x_i(t+1) = \varepsilon(t)x_i(t) + (1 - \varepsilon(t))m_i(t+1). \quad (18)$$

Step 3: Consensus process,

$$z_i(t+1) = \sum_{j \in N_i^m(t) \cup i} h_{ij}(t)z_i(t) - g_i(t), \quad (19)$$

$$g_i(t+1) = \sum_{j \in N_i^m(t) \cup i} h_{ij}(t)g_i(t) + \varepsilon(t)((x_i(t+1)$$

$$- \begin{bmatrix} Ld_i(t) \\ 0 \end{bmatrix} \Big) - \left(x_i(t) - \begin{bmatrix} Ld_i(t) \\ 0 \end{bmatrix} \right)$$

Step 4: Update the dual variable,

$$\zeta_i(t+1) = \varepsilon(t)\zeta_i(t) + (1 - \varepsilon(t))z_i(t+1). \quad (20)$$

Step 5: Go to step 1, until convergence condition satisfied. If converges, get the results $P_{Bi} = x_i(t+1)$, $Q_{Bi} = y_i(t+1)$.

Therefore, the primal variable of BESS unit $i \in N_B$ is $m_i(t) = [P_{Bi}(t), Q_{Bi}(t)]_{2 \times 1}^T$ meanwhile the auxiliary variables $x_i(t), z_i(t)$ and $\theta_i(t)$ will also be the 2×1 vectors. And the primal variables and auxiliary variables of PV unit $i \in N_V$ and FL unit $i \in N_L$ are the same as them of BESS unit. Moreover, each unit sends and receives information from its neighbors over the time-varying directed network and these information, i.e., $[z_i(t), g_i(t)]$ is used to acquire global gradient information by processing consensus steps mentioned in (14). However, the variables $m_i(t), x_i(t)$ and $\zeta_i(t)$ are local variables, which help to solve the optimization problem locally.

4. System voltage stability analysis

This section studies the system performance when distributed algorithms (11), (14) as well as dynamic pricing strategy (9) are adopted in VESS. In order to simplify the analysis and save the space, only the voltage performance of system is investigated in this section. The linearized DistFlow equations for power system with impedance vector $Z = R' + jX'$ can be formulated as follows [41],

$$U(t) = R \cdot P(t) + X \cdot Q(t) + U_0, \quad (21)$$

where U_0 is the system rated voltage and $R = F \cdot R' \cdot F^T$, $X = F \cdot X' \cdot F^T$. And $R = \text{diag}\{R'\}$ and $X = \text{diag}\{X'\}$ are the diagonal matrixes which are symmetric and strictly positive-definite. $P(t)$ and $Q(t)$ are the power injection vector of nodes. The matrix $F = -A^{-1}$ where A is the reduced branch-bus incidence matrix. If the dynamic price is added to the optimization process, equation (21) is reformulated as,

$$U(t) = \underbrace{[R, X] \begin{bmatrix} P(t) \\ Q(t) \end{bmatrix}}_{\Delta R(t)} + U_0 + RE_p \cdot Tr_p(t) + XE_q \cdot Tr_q(t), \quad (22)$$

where matrix $E_p = [ep_{ii}]_{N \times N}$ and $E_q = [eq_{ii}]_{N \times N}$ are the diagonal matrix where $ep_{ii} = -\frac{1}{2ap_i}$ and $eq_{ii} = -\frac{1}{2aq_i}$ and ap_i, aq_i are the parameter of quadratic term of active and reactive power objective function i . The vector $Tr_p(t)$ and $Tr_q(t)$ are the dynamic price vectors of active and reactive power, respectively.

By differentiating (22) we have,

$$\dot{U}(t) = \Delta \dot{R} + RE_p(\alpha_p k_l (U^{ave}(t) - U(t)) + \alpha_p k_p \dot{U}(t)) \quad (23)$$

$$+ XE_q(\alpha_q k_l (U^{ave}(t) - U(t)) + \alpha_q k_p \dot{U}(t)),$$

where α_p, α_q are the parameters of active and reactive power dynamic price, while $U^{ave}(t) = \frac{1}{N} \mathbf{1}^T U(t)$ is the system average voltage. Simplify expression (23) we get,

$$\dot{U}(t) = \underbrace{(I - A_{SP})^{-1} A_{SI}}_{A_S} U(t) + \underbrace{(I - A_{SI})^{-1} A_{SI}}_{B_S} \mu(t) + \Theta, \quad (24)$$

where

$$A_{SP} = -(\alpha_p k_p \cdot RE_p + \alpha_q k_p \cdot XE_q), \quad (25)$$

$$A_{SI} = -(\alpha_p k_l \cdot RE_p + \alpha_q k_l \cdot XE_q),$$

$$\mu(t) = \frac{\mathbf{1} \cdot \mathbf{1}^T}{N} U(t),$$

$$\Theta = (I - A_{SI})^{-1} \Delta \dot{R}(t).$$

In the expression (24) system matrix A_S , and B_S are the key to analyze the system performance. Moreover, Θ is the bounded disturbance of the system which is actually caused by the fluctuation of RES and load demand. For a given system, the physical structure and transmission line parameters are constant and known, i.e., matrixes R, X and E_p, E_q are given. Only the parameters k_l and k_p , which have impacts on system voltage stability, need to be designed. If we assume Θ equals zero, the system voltage stability mainly depends on the eigenvalues of matrix $A_S + B_S \frac{\mathbf{1} \cdot \mathbf{1}^T}{N}$, in other word, it depends on the roots of characteristic equation of matrix $A_S + B_S \frac{\mathbf{1} \cdot \mathbf{1}^T}{N}$. Obviously, the roots are functions of parameters k_l and k_p , thus one can choose some constants for k_l and k_p only to keep the real parts of roots negative. The proposed analysis of system voltage is based on linearized DistFlow equations, which might not explain the exact voltage behaviors. Moreover, virtual reference value could be included into the estimated system average voltage of each node so that node voltages can be guided by the pre-defined virtual value. Thus further study is necessary to analyze the voltage performance when dynamic pricing strategy is included.

5. Simulation results

5.1. System configuration

In order to test the performance of the proposed strategy and method, simulation case studies are tested on a digital simulator (OPAL-RT) which provides real time solutions for VESS model. In this model, as Fig. 1 shows, the bottom physical system, 23-nodes low voltage DNs, which is derived from the real case from a southwest town of China, contains four BESS, five FL, eight PV and InFL. While the upper communication network with 18 nodes is a set of time-varying directed graphs which share information locally for each controllable unit. Besides, the physical constraints of lead-acid battery based BESS, PV and FL are considered in this model, where constraints of power capacities, SoC are adopted in the bottom physical layer. Line impedance is $0.3811 + j0.1514 \Omega/km$ and the total length of branch lines in VESS is about 2.8 km. Moreover, the capacities of BESS, PV are listed in Table 1, while the parameters of objective function are listed in Tables 2–4. At the initial time, the system works in a balanced state.

5.2. Power management of VESS without dynamic price

The simulation results are shown in Fig. 3 and Fig. 4, and Fig. 5. In Fig. 3 (a) and (b), BESS and PV generate power smoothly, and between 8:00 a.m. to 8:00 p.m. the outputs of PV vary in a range of 5–85 kW while the outputs of BESS are between –50 and +50 kW.

Table 1
Capacities of BESS, PV and FL of VESS.

Sources	p^{max}	p^{min}	SoC(0)%	$\cos(\varphi)$
PV ₁	60 kW	0 kW	—	0.9
PV ₂	60 kW	0 kW	—	0.9
PV ₃	60 kW	0 kW	—	0.9
PV ₄	85 kW	0 kW	—	0.9
PV ₅	45 kW	0 kW	—	0.9
PV ₆	66 kW	0 kW	—	0.9
PV ₇	63 kW	0 kW	—	0.9
PV ₈	66 kW	0 kW	—	0.9
BESS ₁	50 kW	-50 kW	60	0.9
BESS ₂	50 kW	-50 kW	62	0.9
BESS ₃	50 kW	-50 kW	63	0.9
BESS ₄	50 kW	-50 kW	64	0.9

Table 2
Parameters of objective functions.

Sources	α_i	β_i	a_{Bi}	b_{Bi}
BESS ₁	0.032	1.5	0.1	0.25
BESS ₂	0.028	2	0.1	0.22
BESS ₃	0.034	1.8	0.1	0.23
BESS ₄	0.04	1.3	0.1	0.26

Table 3
Parameters of objective functions.

Sources	a_i	b_i	a_{Vi}	b_{Vi}
PV ₁	1	0.11	1	0.13
PV ₂	1	0.13	1	0.15
PV ₃	1	0.12	1	0.14
PV ₄	1	0.10	1	0.12
PV ₅	1	0.09	1	0.11
PV ₆	1	0.14	1	0.17
PV ₇	1	0.15	1	0.16
PV ₈	1	0.11	1	0.18

Table 4
Parameters of objective functions.

Sources	η_i	ν_i	a_{Fi}	b_{Fi}
FL ₁	0.28	5.1	1	0
FL ₂	0.29	5.5	1	0
FL ₃	0.30	5.2	1	0
FL ₄	0.31	5.3	1	0
FL ₅	0.26	5.0	1	0

Besides, the demand of FL, PCC power are shown in Fig. 5. According to the results shown in Fig. 4, it can be seen that system voltage is unsatisfying and is changing from 0.93 to 1.16 p.u which is far beyond the limits from 0.95 to 1.05 p.u. From Fig. 5 (a) and (b), we see that the demand of FL are varying from 5 to 31 kW while the active PCC power changes between 0 and 10 kW except the time period from 13:00 to 17:00pm. From 13:00 to 17:00pm, VESS injects power into the grid since the outputs of PV are larger than the load demand and power absorbed by BESS. Thus PCC power is far away from 10 kW and its maximal power reaches -50 kW at time 16:00pm. While the reactive power of PCC unit is stay close to 0 kVar, except the slight increase during 13-17:00pm.

5.3. Power management of VESS with dynamic price

The simulation results are shown in Fig. 6, to Fig. 11. Fig. 6 (a), (b) show the active power of PV and BESS, respectively, while Fig. 8 (a)

and (b) are the load demand of FL and PCC power. From Fig. 6 (a), we know that the outputs of PV are different compared from the results in Fig. 3 (a) when dynamic price term is added. Certainly, the active outputs power of PV are changing between 0 and 72 kW while the reactive power is between -15 and 10 kVar (see Fig. 7).

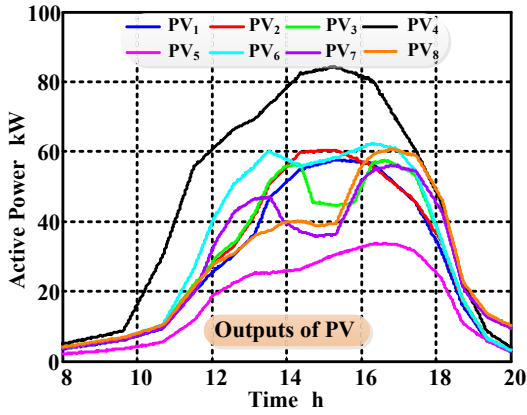
PV units will increase outputs when their voltages are lower than the system average voltage, such as the reactive outputs of PV₁, PV₄, PV₆ and PV₇ shown in Fig. 7(a) from 8:00 to 11:00 a.m. On the contrary, PV units will decrease outputs when their voltages are higher than the system average voltage, such as the decreasing reactive outputs of PV₂, PV₃, PV₄ and PV₅ shown in Fig. 7(a). For example, node voltages at PV₆, PV₇ and PV₈ (represented by Um_{15} , Um_{16} and Um_{17}) are driven into the normal range, when PV₆, PV₇ and PV₈ generate negative reactive power. However, the outputs of PV always meet the constraints. From the results, we know that the outputs of PV are changing with both system voltages and economic costs.

While the outputs of BESS, shown in Figs. 6(b) and Fig. 7(b), vary from the results in Fig. 3(b), i.e., the charging power of BESS₂ and BESS₃ shown in Fig. 7(b) is smaller than them in Fig. 3(b) because voltages of BESS₂ and BESS₃ are below the lower voltage limit such that BESS₂ and BESS₃ will provide reactive power (shown in Fig. 7(a)) in order to drive voltage into the normal range. In this way, with the constraints of power factor, the active power of BESS₂ and BESS₃ are reduced compared with them in Fig. 3(b). Thus, the system voltage is regulated when dynamic pricing is added to the economic power dispatch problem (7).

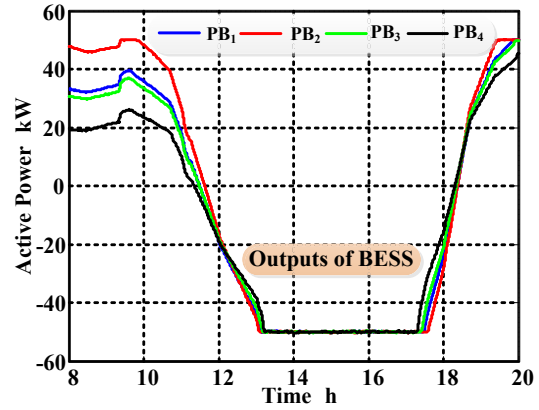
The load demands of FL and PCC power, which are also changing within the limits (5-31 kW), shown in Fig. 8, vary according to the system voltage condition. The load demands of FL decrease when system voltage is low, and vice versa. It can be seen in Fig. 8(a) that load demands of FL₁, FL₂, FL₃, FL₄ are lower than the demands of them in Fig. 6(a) between the duration from 8:00 a.m. to 12:00 p.m. and from 18:00 to 20:00 p.m. However, during the time 13 to 17:00 p.m., the load demands of FL reaches their maximal points when system voltage is high. The PCC active power shown in (b) varies smoother when compared with the results in Fig. 6(b), meanwhile the reactive power is changing from -25 to 25 kVar. Therefore, when dynamic price is added, the outputs of PV, BESS and demand of FL are changing not only according to their economical cost but also system voltage condition.

The system voltage, dynamic price are shown in Fig. 9(a) and (b). In Fig. 9(a), the voltages of PV, BESS and FL are $Um_1, \dots, Um_8, Um_9, \dots, Um_{12}$ and Um_{13}, \dots, Um_{17} , respectively. From Fig. 9(a), we know that system voltages vary in the normal range, i.e., system voltages are between 0.95 and 1.05 p.u, while the dynamic price of each unit is changing according to the system voltages to adjust the outputs of PV and BESS, shown in Fig. 9(b). When system voltage is high, its local dynamic price causes the variation of node reactive and active injection power. In other word, dynamic price in model (3) and (5) enables PV units to adjust their outputs. Dynamic price of BESS units have the similar purpose with that in PV units.

In addition, compared with results in Fig. 3(a), (b) and Fig. 5(a), the curtailed power of PV, BESS and FL are shown in Fig. 10(a), (b) and Fig. 11(a). From Fig. 10(a), the curtailed powers of PV are between 0 and 22 kW and the amount of curtailed power of PV₈ is the largest while the curtailed power of PV₅ is the smallest. The voltage of PV₈ is the highest, in terms of dynamic price, the curtailed power of PV₈ is the largest among all PV sources. While the differences of BESS powers are varying between -55 and 30 kW (shown in Fig. 11(a)) and the differences of FL power are changing from -5 to 10 kW (shown in Fig. 10(b)). Besides, the SoC of BESS is within the limit, i.e., $0.15 \leq SoC_{i \in N_b}(t) \leq 0.85$, shown in Fig. 11(c). All of these power changes are induced by the system voltage-based dynamic



(a)



(b)

Fig. 3. Simulation results without dynamic price (Left, (a); Right, (b)). (a) Operation condition of PV. (b) Operation condition of BESS.

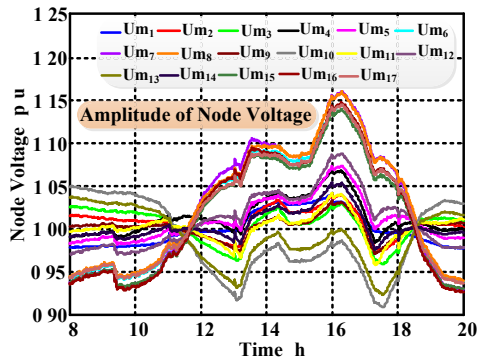


Fig. 4. Simulation results without dynamic price. Fluctuation of system voltage.

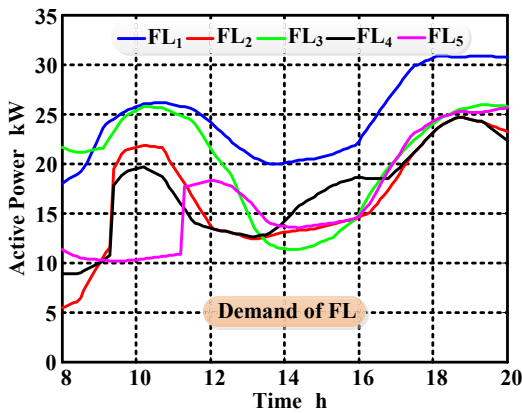
price. With the proposed dynamic price, each unit in VESS adjusts its power condition depending on both economical cost and system voltage condition.

To conclude, the dynamic pricing rules have the impacts on the fluctuation of system voltage. In detail, dynamic price enable PV, BESS and FL units in VESS to adjust output power (active and reactive power) according to the system voltage. When node voltages of PV nodes are high, PV units will generate negative reactive

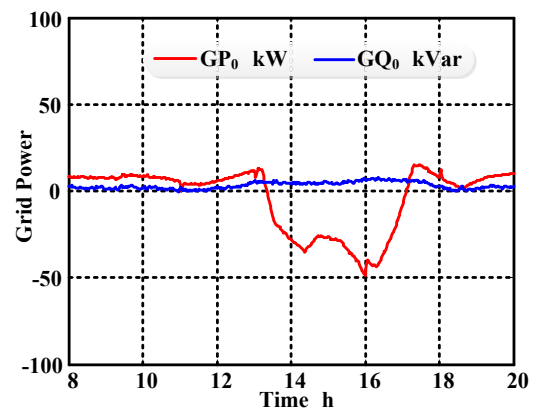
power and curtail active power in order to drive voltage into the normal range. When voltages at PV nodes are low, PV units will generate positive reactive power, however, PV units will not provide extra active power, since it is constrained by sunlight irradiation. For BESS unit, BESS will generate less active power and reactive power (or maybe negative reactive power) when its node voltage are high, and vice versa. When voltages at FL nodes are low, the demand of FL will decrease, see in Fig. 10(b), from which we can see the curtailed power of FL is positive (FL_3 and FL_1) from 8:00am to 13:pm. That is, in order to adjust node voltages, FL decreases its power consumption. Overall, VESS power is shared among BESS, PV and FL units according to the operation costs and voltage condition.

6. Conclusion

This paper presented a distributed optimization model for VESS real-time power management considering dynamic price, to minimize system costs and to drive system voltage into the normal range. Considering system voltage performance and system power economic sharing, the distributed dynamic pricing strategies were incorporated into the model. In order to derive distributed solution for VESS, a set of distributed algorithms with dynamic weights, over the time-varying communication networks were designed to form dynamic price and solve VESS optimization model. The 23-bus



(a)



(b)

Fig. 5. Simulation results without dynamic price (Left, (a); Right, (b)). (a) Demand condition of FL. (b) Power condition of PCC unit.

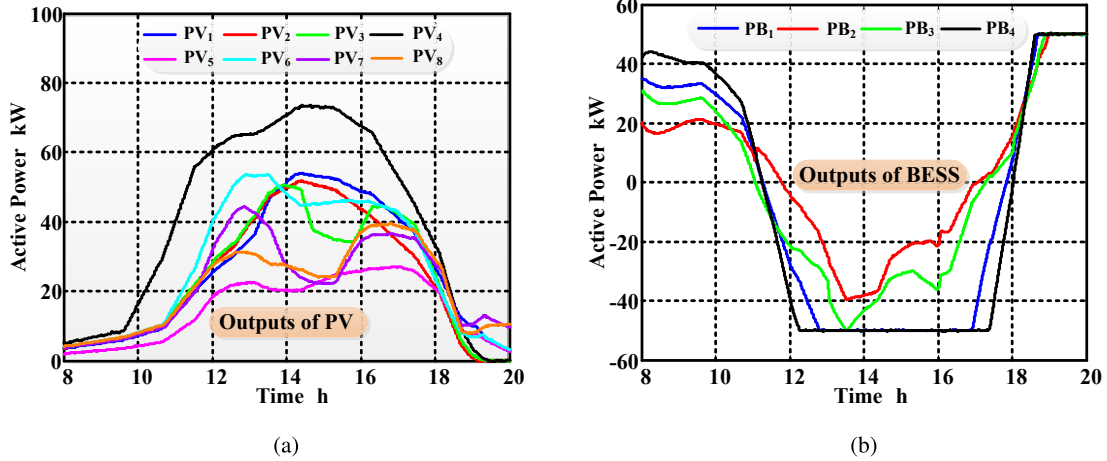


Fig. 6. Simulation results when dynamic price is added (Left, (a); Right, (b)). (a) Active Power of PV. (b) Active Power of BESS. (c) Load demand of FL. (d) Reactive Power of PV. (e) Reactive Power of BESS. (f) Power of PCC.

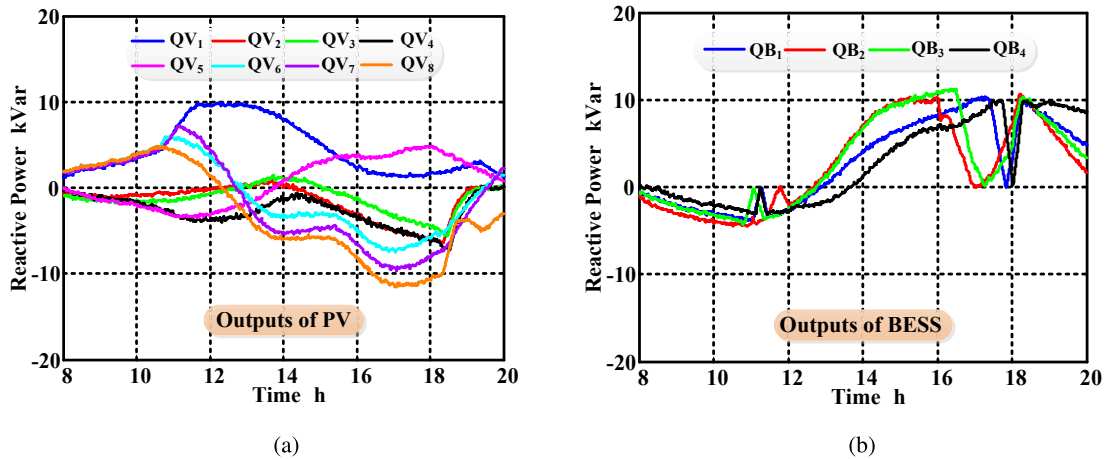


Fig. 7. Simulation results when dynamic price is added (Left, (a); Right, (b)). (a) Reactive Power of PV. (b) Reactive Power of BESS.

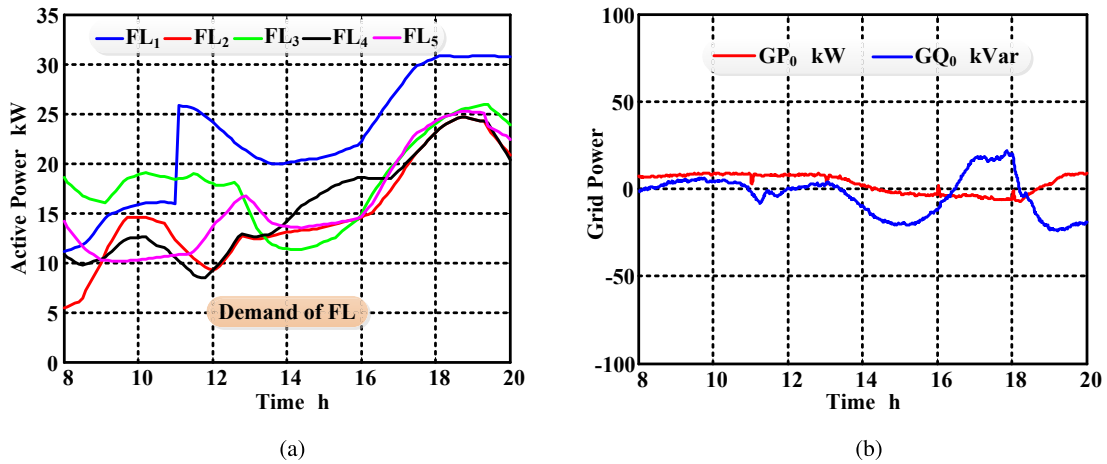


Fig. 8. Simulation results when dynamic price is added (Left, (a); Right, (b)). (a) Load demand of FL. (b) Active Power of BESS.

VESS simulation platform, which was derived from the real DN, was built on a real time simulator (OPAL-RT OP5600) to evaluate the proposed dynamic pricing and optimization model. Simulation

results demonstrated that as the node voltages at RES increase, the local dynamic price signals decrease, while RES curtails its active power and absorbs reactive power. Meanwhile, BESS charging

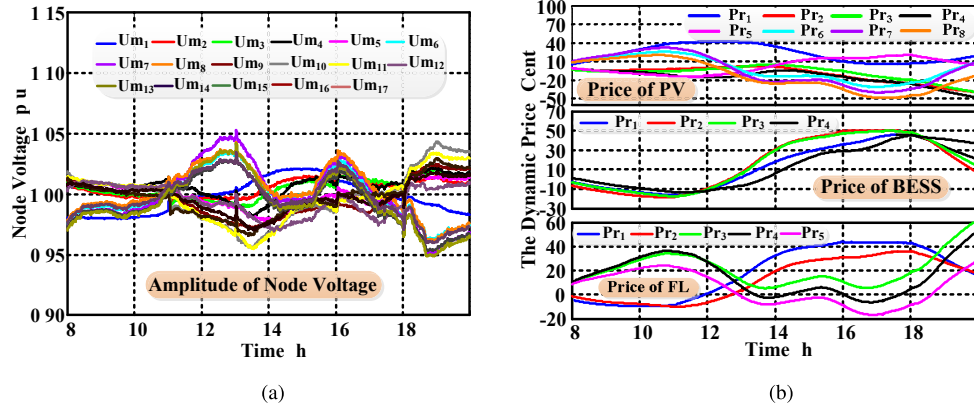


Fig. 9. Simulation results with dynamic price (Left, (a); Right, (b)). (a) is the system voltages. (b) is the dynamic price of each unit.

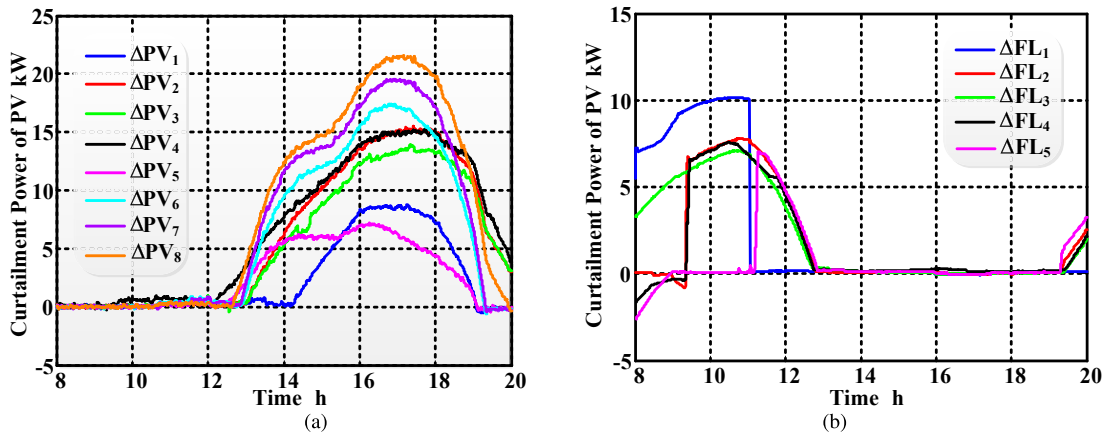


Fig. 10. Simulation results with dynamic price (Left, (a); Right, (b)). (a) The curtailed power of PV. (c) the curtailed power of FL.

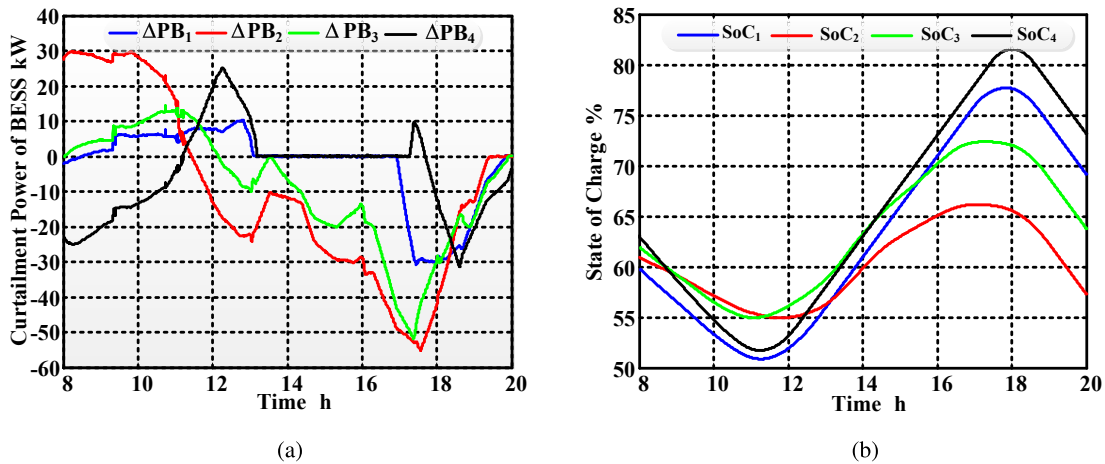


Fig. 11. Simulation results with dynamic price (Left, (a); Right, (b)). (a) is the curtailed power of BESS. (b) is the variation of SoC of BESS.

active and reactive power increase when node voltages increases. For FL, demand power increases when node voltage increases. In other word, the results show operation costs are minimized, and system voltages are driven into the normal range by curtailing rational PV active power and injecting reasonable reactive power. Furthermore, simulation results show that operation condition of VESS depends both on node voltages and economic costs, namely,

both system voltages and economic parameters decide VESS power sharing behavior. Our future research work is to design robust dynamic pricing strategy that can adapt the disturbance caused by fluctuation of inflexible loads.

Declaration of competing interest

The authors declare that they have no known competing financial interests or personal relationships that could have appeared to influence the work reported in this paper.

Acknowledgments

This work was supported in part by the National Natural Science Foundation of China (under Grant No. 61105125 & No. 51177177), in part by the National "111" Project of China (under Grant No. B08036) and in part by the Science and Technology Project of State Grid Zhejiang Electric Power Company (under Grant No. 5211W4180001).

Appendix A

7.1. Convergence Analysis of Voltage Estimation Algorithm

We can rewrite our algorithm (11) as

$$J(t+1) = W(t)J(t), \quad (26)$$

$$\text{where } J(t+1) = [U^{ave}(t+1), V(t+1)], \quad W(t) = \begin{bmatrix} I, & -\frac{1}{2}I; \\ -H(t), & I+H(t) \end{bmatrix}_{2N \times 2N}.$$

In order to investigate the property of matrix $I+H(t)$ and discover the relationship between $I+H(t)$ and $W(t)$. The following lemmas are provided.

Lemma 1. Assume that $I+H(t)$ is a set of sequence of column stochastic matrices, then the spectral radius of matrix $I+H(t)$ is $\rho(I+H(t)) \leq 1$ where the equation stands for the $\kappa(I+H(t)) = \kappa$ (κ is a vector with same entries). Moreover, when $t \rightarrow \infty$, we get $I+H(t) = H'$, where H' is a double stochastic matrix.

Proof. The graph $G(t)$ is a connected graph, where the non-negative column stochastic matrix $I+H(t)$ is the weight matrix. Thus we know that one of the eigenvalues of $I+H(t)$ is 1 and its corresponding vector is κ . And the magnitudes of other eigenvalues of $I+H(t)$ are all less than 1. Thus the spectral radius of matrix $I+H(t)$ is $\rho(I+H(t)) \leq 1$. According to the proof of Theorem 4.14 of [42], it can be known that the equation $I+H(t)|_{t \rightarrow \infty} = H'$ is reasonable.

Lemma 2. The spectral radius of matrix $W(t)$ is $\rho(W(t)) \leq 1$ and one is its eigenvalue.

Proof. Assume that the eigenvalue of matrix $I+H(t)$ is $\beta(t)$ and its corresponding eigenvectors are $\nu(t)$. Thus, $(\beta(t)-1)$ and $\theta(t)$ are the eigenvalue and its eigenvector of matrix $H(t)$, respectively. Let $[\theta(t), \pi(t)]$ and $\gamma(t)$ be the eigenvector and eigenvalue of matrix $W(t)$, then we will get following expression,

$$\begin{cases} \theta(t) - \frac{1}{2}\pi(t) = \gamma(t)\nu(t), \\ -H(t)\theta(t) + (I+H(t))\pi(t) = \gamma(t)\pi(t). \end{cases} \quad (27)$$

Simplify the equation (27), we get,

$$2\gamma^2(t) - 2\gamma(t)(\beta(t)+1) + \beta(t)+1 = 0. \quad (28)$$

Hence, the eigenvalue of matrix $W(t)$ is,

$$\gamma(t) = \frac{1}{2} \left(1 + \beta(t) \pm \sqrt{\beta(t)^2 - 1} \right). \quad (29)$$

From (29), we know that $\gamma_1(t) = 1(\beta_1(t) = 1)$. Next, it can be

proved that $\gamma(t) = \frac{1}{2}(1 + \beta(t)) \pm j\frac{1}{2}\sqrt{1 - \beta^2(t)}$ since $\beta^2(t) \leq 1$. Therefore, the spectral radius $\rho(W(t)) = |\gamma(t)| = \frac{1}{4}(1 + \beta(t))^2 + \frac{1}{4}(1 - \beta^2(t)) = \frac{1}{2}(1 + \beta(t)) \in (0, 1]$. This completes the proof.

In terms of lemma 2, we know that system (14) is stable. Next, the consensus performance of algorithm (14) is studied. According to the lemma 2 of [43], it can be proved that the algorithm (14) achieves consensus asymptotically, i.e., $U_1^{ave}(\infty) = \dots = U_j^{ave}(\infty) = \dots = U_N^{ave}(\infty)$, $V_1(\infty) = \dots = V_j(\infty) = \dots = V_N(\infty)$. In light of lemma 1, we know that the column summation of matrix $H(t)$ is zero, which guarantees the expression,

$$\sum_{i=1}^N U_i^{ave}(t+1) \quad (30)$$

$$= \left(V_1(t) \sum_{j=1}^N H_{j,1}(t) + \dots + V_n(t) \sum_{j=1}^N H_{j,n}(t) \right)$$

$$+ \left(U_1^{ave}(t) \sum_{j=1}^N H_{j,1}(t) + \dots + U_n^{ave}(t) \sum_{j=1}^N H_{j,n}(t) \right)$$

$$+ \sum_{i=1}^N U_i^{ave}(t) = \sum_{i=1}^N U_i^{ave}(t) = \dots = \sum_{i=1}^N U_i^{ave}(0).$$

Therefore, the expression $U_1^{ave}(\infty) = \dots = U_j^{ave}(\infty) = \dots = U_N^{ave}(\infty) = \frac{1}{N} \sum_{i=1}^N U_i^{ave}(0)$ holds. Combine Lemma 1 and Lemma 2, the proof of Theorem 1 is finished.

7.2. Optimal Analysis of Proposed Distributed Algorithm

Before providing the proof of Theorem 2, we first analyze the convergence property of unconstrained algorithm, which are formulated as,

$$\begin{cases} z_i(t+1) = \sum_{j \in N_i^m(t) \cup i} h_{ij}(t) z_j(t) - g_i(t), \\ g_i(t+1) = \sum_{j \in N_i^m(t) \cup i} h_{ij}(t) g_j(t) \\ + \varepsilon(t) (\Delta f_i(z_i(t+1)) - \Delta f_i(z_i(t))), \end{cases} \quad (31)$$

where $\Delta f_i(z_i(k+1))$ is the gradient of the objective function. Rewrite the (31) as the compact form, we get,

$$\begin{bmatrix} Z(t+1) \\ g(t+1) \end{bmatrix} = \begin{bmatrix} I+H(t) & -I \\ \mathbf{0} & I+H(t) \end{bmatrix}_{2N \times 2N} \cdot \begin{bmatrix} Z(t) \\ g(t) \end{bmatrix} + \varepsilon(t) \underbrace{(\Delta \hat{F}(t+1) - \Delta \hat{F}(t))}_{\Delta G(t+1)}, \quad (32)$$

where $\Delta \hat{F}(t)$ is the gradient vector. Let the tuning parameter $\varepsilon(t) = 0$ and $\hat{H}(t) = I+H(t)$, $Zg(t) = [Z(t), g(t)]^T$, the expression (32) ll be,

$$\begin{bmatrix} Z(t+1) \\ g(t+1) \end{bmatrix} = \underbrace{\begin{bmatrix} \hat{H}(t)-I \\ \mathbf{0} \hat{H}(t) \end{bmatrix}_{2N \times 2N}}_{K(t)} \cdot \begin{bmatrix} Z(t) \\ g(t) \end{bmatrix}. \quad (33)$$

Thus, apply (33) recursively and yields,

$$Zg(t+1) = \underbrace{[K(t)K(t-1)\cdots K(0)]}_{\Gamma_{K(t)}(t:0)} Zg(0). \quad (34)$$

Following theorem 3 is proposed to analyze the property of matrix $\Gamma_{K(t)}(t:0)$.

Theorem 3. The recursive product $\Gamma_{K(t)}(t:0)$ of matrix $K(t)$ reaches K' when $t \rightarrow \infty$, where matrix K' is,

$$K' = \begin{bmatrix} \frac{1 \cdot 1^T}{N} & -t \frac{1 \cdot 1^T}{N} \\ 0 & \frac{1 \cdot 1^T}{N} \end{bmatrix}_{2N \times 2N}. \quad (35)$$

Proof. According to the definition of product $\Gamma(t:0)$, it yields,

$$\Gamma_{K(t)}(t:0) = \begin{bmatrix} \tilde{H}(t)\tilde{H}(t-1)\cdots\tilde{H}(0) & -\Lambda(t) \\ 0 & \tilde{H}(t)\tilde{H}(t-1)\cdots\tilde{H}(0) \end{bmatrix} \quad (36)$$

and,

$$\Lambda(t) = \sum_{i=1}^t \Gamma(t:0, i), \quad (37)$$

where,

$$\begin{aligned} \Gamma_{\tilde{H}(t)}(t:0, i) & \quad (38) \\ &= \tilde{H}(t)\tilde{H}(t-1)\cdots\tilde{H}(t-i+1)\tilde{H}(t-i-1)\cdots\tilde{H}(0) \\ &= \Gamma_{\tilde{H}(t)}(t:i+1)\Gamma_{\tilde{H}(t)}(t-i-1:0). \end{aligned}$$

According to the Lemma 3 of [40], we get $|\tilde{H}(t)\tilde{H}(t-1)\cdots\tilde{H}(s) - \frac{1 \cdot 1^T}{N}| \leq C\delta^{t-s+1}$, where C is a positive constant while $\delta \in (0, 1)$. Therefore, $\tilde{H}(t)\tilde{H}(t-1)\cdots\tilde{H}(0) = \frac{1 \cdot 1^T}{N}$, and $\Lambda(t) = t \cdot \frac{1 \cdot 1^T}{N}$, when $t \rightarrow \infty$.

In terms of theorem 3, the algorithm (33) is one kind of augmented consensus algorithms which leads $z_N(t) = \cdots = z_1(t)$ and $g_N(t) = \cdots = g_1(t)$ when $t \rightarrow \infty$. If the tuning parameter $\varepsilon(t) = \frac{1}{t+1}$ and the gradient vector $\Delta\hat{F}(t)$ is bounded, the following corollary is deduced.

Corollary. Given any variables $Z_i(t), g_i(t)$ and bounded $\Delta\hat{F}(t)$ for each unit on communication network $G(N, \varepsilon(t), A(t))$, we have,

$$\lim_{t \rightarrow \infty} \left| g_i(t) - \frac{1}{N} \sum_{j=1}^N g_j(t) \right| = 0, \quad (39)$$

$$\lim_{t \rightarrow \infty} \left| Z_i(t) - \frac{1}{N} \sum_{j=1}^N Z_j(t) \right| = 0. \quad (40)$$

Proof. The expression (32) becomes,

$$Zg(t+1) = [K(t)K(t-1)\cdots K(0)]Zg(0) \quad (41)$$

$$- \sum_{l=1}^{t-1} (K(t-1)\cdots K(s+1))\lambda(l)\Delta G(l) - \lambda(t)\Delta G(t), (t \geq l).$$

While for vector $g(t)$, we have,

$$g(t+1) = [\tilde{H}(t)\tilde{H}(t-1)\cdots\tilde{H}(0)]g(0) \quad (42)$$

$$- \sum_{l=1}^{t-1} (\tilde{H}(t-1)\cdots\tilde{H}(s+1))\lambda(l)g(l) - \lambda(t)g(t), (t \geq l).$$

Thus, using Holder's inequality, for (42), it yields,

$$\left| g_i(t) - \frac{1}{N} \sum_{j=1}^N g_j(t) \right| = \left| [\tilde{H}(t)\tilde{H}(t-1)\cdots\tilde{H}(0)]g(0) \right|_i \quad (43)$$

$$- \frac{1}{N} \sum_{j=1}^N g_j(0) - \sum_{l=1}^{t-1} \lambda(l) [\tilde{H}(t-1)\cdots\tilde{H}(l+1)]g(l)_i$$

$$+ \frac{1}{N} \sum_{l=0}^{t-1} \lambda(l) \sum_{i=1}^N g_i(l) \Big|$$

$$\leq \max_j \left| [\tilde{H}(t)\tilde{H}(t-1)\cdots\tilde{H}(0)]_{ij} - \frac{1}{N} \right| \times g(0)_1$$

$$+ \sum_{l=0}^{t-1} \varepsilon(l) g(l)_1 \max_j \left| [\tilde{H}(t-1)\cdots\tilde{H}(l+1)]_{ij} - \frac{1}{N} \right|$$

$$\leq B\delta^t g(0)_1 + \sum_{l=0}^{t-1} B\delta^{t-l-1} \varepsilon(l) g(l)_1,$$

Therefore, when $t \rightarrow \infty$, expression (39) holds. Similarly, for (40), we have,

$$\left| Z_i(t) - \frac{1}{N} \sum_{j=1}^N Z_j(t) \right| = \left| [\Gamma(t:0)]Z(0) \right|_i - \frac{1}{N} \sum_{j=1}^N Z_j(0) \quad (44)$$

$$- \sum_{l=1}^{t-1} \varepsilon(t) [\Gamma(t-1:l+1)]_i + \frac{1}{N} \sum_{l=0}^{t-1} \varepsilon(l) \sum_{i=1}^N Z_i(l) \Big|$$

$$\leq \max_j \left| [\Gamma(t:0)]_{ij} - \frac{1}{N} \right| \times \|Z(0)\|_1$$

$$+ \sum_{l=0}^{t-1} \varepsilon(l) \|Z(l)\|_1 \max_j \left| [\Gamma(t:l+1)]_{ij} - \frac{1}{N} \right|$$

$$\leq (t+1)B_1 \left(\delta^t Z(0)_1 + \sum_{l=0}^{t-1} \delta^{t-l-1} \varepsilon(l) Z(l)_1 \right).$$

We get $\lim_{t \rightarrow \infty} (t+1)\delta^t = 0$ since $\delta \in (0, 1)$. Therefore, the formula (40) and (39) are proved.

From the above corollary, it can be seen that variables $z_i(t), g_i(t)$ synchronize even when the tuning parameter $\varepsilon(t) = \frac{1}{t+1}$. Besides, the objective function $F(t)$ is convex and its gradient is bounded, it can also be proved that $\lim_{t \rightarrow \infty} |F(z(t)) - F(z^*)| = 0$, since $\sum_{t=1}^{\infty} \varepsilon(t) = \infty$, $\sum_{t=1}^{\infty} \varepsilon(t)^2 \leq \infty$, where $F(z^*) = \min_{z \in \Omega} F(z(t))$.

In order to save the space, the detailed mathematical proof of constrained optimization problem is omitted here. However, the analysis is provided. The optimization problem with inequality and equality constraints can be formulated as,

$$\begin{cases} \min_z F(z) = \sum_{i=1}^N f_i(z_i), \\ s.t. z_1(t) + \dots + z_i(t) + \dots + z_N(t) = Zeq, \\ z_{i,min} \leq z_i(t) \leq z_{i,max}, i = 1, \dots, N, \end{cases} \quad (45)$$

Thus, the Lagrangian function of (45) is expressed as,

$$L(z(t), \zeta(t)) = \sum_{i=1}^N f_i(z_i(t)) - \zeta(t) \left(\sum_{i=1}^N z_i(t) - Zeq \right), \quad (46)$$

where $\zeta(t)$ is the dual variable. And the Lagrangian dual problem of (46) is formulated as,

$$\begin{aligned} & \max_{\zeta(t)} \phi(\zeta(t)) \\ & = \max_{\zeta(t)} \sum_{i=1}^N \underbrace{\left(\min_{z_i \in [z_{min,i}, z_{max,i}]} F_i(z_i) - \zeta(t)(z_i - Zeq_i) \right)}_{\phi_i(\zeta(t))}, \end{aligned} \quad (47)$$

where $Zeq_i = Ld_i$ is the load demand of unit i . For dual variable $\zeta(t)$, the dual problem (47) is an unconstrained optimization problem since there is no constraint to the dual variable ζ . Therefore, the gradient of dual problem (47) for each unit i is $\Delta F_i(t) = - (z_i(t) - Zeq_i)$. For an unconstrained optimization problem, the proposed corollary guarantees the optimality. This completes the proof.

References

- [1] Cao M, Wang H, Li K, Wu Z, Sun L. Dynamic coordination optimization for active distribution network considering energy storage system. 2020. p. 675–88.
- [2] Abbott D. "Keeping the energy debate clean: How do we supply the world's energy needs? Proc IEEE 2010;98(1):42–66.
- [3] Guerrero JM, Chandorkar M, Lee T, Loh PC. "Advanced control architectures for intelligent microgrids—Part I: Decentralized and hierarchical control. IEEE Trans Ind Electron 2013;60(4):1254–62.
- [4] Lasseter RH, Paigi P. Microgrid: a conceptual solution June 2004;6:4285–90. Vol.6.
- [5] Shaaban MF, Mohamed S, Ismail M, Qaraqe KA, Serpedin E. Joint planning of smart ev charging stations and dgs in eco-friendly remote hybrid microgrids. IEEE Transactions on Smart Grid Sep. 2019;10(5):5819–30.
- [6] Tang C, Zhang W, Liu R. Alternating iterative method for congestion management of microgrid integrated distribution network. Sep. 2017. p. 471–6.
- [7] Farrokhbadi M, Cañizares CA, Simpson-Porco JW, Nasr E, Fan L, Mendoza-Araya PA, Tonkoski R, Tamrakar U, Hatzigaryriou N, Lagos D, Wies RW, Paolone M, Liserre M, Meegahapola L, Kabalan M, Hajimiragha AH, Peralta D, Elizondo MA, Schneider KP, Tuffner FK, Reilly J. Microgrid stability definitions, analysis, and examples. IEEE Transactions on Power Systems Jan 2020;35(1):13–29.
- [8] Tan Z, Li X, He L, Li Y, Huang J. Primary frequency control with bess considering adaptive soc recovery. International Journal of Electrical Power & Energy Systems 2020;117:105588.
- [9] Zeraati M, Hamedani Golshan ME, Guerrero JM. Distributed control of battery energy storage systems for voltage regulation in distribution networks with high pv penetration. IEEE Transactions on Smart Grid July 2018;9(4):3582–93.
- [10] Engels J, Claessens B, Deconinck G. Optimal combination of frequency control and peak shaving with battery storage systems. IEEE Transactions on Smart Grid; 2019. p. 1.
- [11] Amrollahi MH, Bathaee SMT. Techno-economic optimization of hybrid photovoltaic/wind generation together with energy storage system in a stand-alone micro-grid subjected to demand response. Applied energy 2017;202:66–77.
- [12] Casals LC, Barbero M, Corchero C. Reused second life batteries for aggregated demand response services. Journal of cleaner production 2019;212:99–108.

- [13] Karthikeyan N, Pillai JR, Bak-Jensen B, Simpson-Porco JW. Predictive control of flexible resources for demand response in active distribution networks. IEEE Transactions on Power Systems July 2019;34(4):2957–69.
- [14] Choi J, Choi I, Ahn G, Won D. Advanced power sharing method to improve the energy efficiency of multiple battery energy storages system. IEEE Transactions on Smart Grid March 2018;9(2):1292–300.
- [15] Zhu Y, Zhao D, Li X, Wang D. Control-limited adaptive dynamic programming for multi-battery energy storage systems. IEEE Transactions on Smart Grid July 2019;10(4):4235–44.
- [16] Obaid ZA, Cipcigan L, Muhssin MT, Sami SS. Control of a population of battery energy storage systems for frequency response. International Journal of Electrical Power & Energy Systems 2020;115:105463.
- [17] Cheng M, Sami SS, Wu J. Benefits of using virtual energy storage system for power system frequency response. Applied energy 2017;194:376–85.
- [18] Ji Y, Xu Q, Luan K, Yang B. Virtual energy storage model of air conditioning loads for providing regulation service. Energy Reports 2020;6:627–32.
- [19] Cherukuri SHC, Saravanan B. Hybrid energy management strategy for residential consumers using virtual and actual storage systems. Journal of Energy Storage 2019;25:100894.
- [20] Jin X, Mu Y, Jia H, Wu J, Jiang T, Yu X. Dynamic economic dispatch of a hybrid energy microgrid considering building based virtual energy storage system. Applied Energy 2017;194:386–98 [Online]. Available: <http://www.sciencedirect.com/science/article/pii/S0306261916310212>.
- [21] Huang Y, Lan H, Hong Y-Y, Wen S, Fang S. Joint voyage scheduling and economic dispatch for all-electric ships with virtual energy storage systems. Energy 2020;190:116268.
- [22] Congedo PM, Baglivo C, Carrieri L. Hypothesis of thermal and mechanical energy storage with unconventional methods. Energy Conversion and Management 2020;218:113014 [Online]. Available: <http://www.sciencedirect.com/science/article/pii/S0196890420305586>.
- [23] Wang Y, Syed MH, Guillo-Sansano E, Xu Y, Burt GM. Inverter-based voltage control of distribution networks: A three-level coordinated method and power hardware-in-the-loop validation. IEEE Transactions on Sustainable Energy 2020;11(4):2380–91.
- [24] Ju L, Tan Z, Yuan J, Tan Q, Li H, Dong F. A bi-level stochastic scheduling optimization model for a virtual power plant connected to a wind-photovoltaic-energy storage system considering the uncertainty and demand response. Applied Energy 2016;171:184–99 [Online]. Available: <http://www.sciencedirect.com/science/article/pii/S0306261916303312>.
- [25] Vahedipour-Dahraie M, Rashidzadeh-Kermani H, Anvari-Moghaddam A, Siano P. Risk-averse probabilistic framework for scheduling of virtual power plants considering demand response and uncertainties. International Journal of Electrical Power & Energy Systems 2020;121:106126 [Online]. Available: <http://www.sciencedirect.com/science/article/pii/S0142061519341122>.
- [26] Liu Y, Li Y, Gooi HB, Jian Y, Xin H, Jiang X, Pan J. Distributed robust energy management of a multimicrogrid system in the real-time energy market. IEEE Transactions on Sustainable Energy Jan 2019;10(1):396–406.
- [27] Duan J, Chow M. A novel data integrity attack on consensus-based distributed energy management algorithm using local information. IEEE Transactions on Industrial Informatics March 2019;15(3):1544–53.
- [28] Asad R, Kazemi A. A novel distributed optimal power sharing method for radial dc microgrids with different distributed energy sources. Energy 2014;72:291–9 [Online]. Available: <http://www.sciencedirect.com/science/article/pii/S0360544214006021>.
- [29] Radhakrishnan BM, Srinivasan D. A multi-agent based distributed energy management scheme for smart grid applications. Energy 2016;103:192–204 [Online]. Available: <http://www.sciencedirect.com/science/article/pii/S0360544216301797>.
- [30] Li Q, Gao M, Lin H, Chen Z, Chen M. Mas-based distributed control method for multi-microgrids with high-penetration renewable energy. Energy 2019;171:284–95 [Online]. Available: <http://www.sciencedirect.com/science/article/pii/S0360544218325416>.
- [31] Nikmehr N. Distributed robust operational optimization of networked microgrids embedded interconnected energy hubs. Energy 2020;199:117440 [Online]. Available: <http://www.sciencedirect.com/science/article/pii/S0360544220305478>.
- [32] de Azevedo R, Cintuglu MH, Ma T, Mohammed OA. Multiagent-based optimal microgrid control using fully distributed diffusion strategy. IEEE Transactions on Smart Grid 2017;8(4):1997–2008.
- [33] Ferreira PDF, Carvalho PMS, Ferreira LAFM, Ilic MD. Distributed energy resources integration challenges in low-voltage networks: Voltage control limitations and risk of cascading. IEEE Transactions on Sustainable Energy 2013;4(1):82–8.
- [34] Kushwaha V, Pindoriya NM. Very short-term solar pv generation forecast using sarima model: A case study. Dec 2017. p. 430–5.
- [35] Dall'Anese E, Dhople SV, Giannakis GB. Photovoltaic inverter controllers seeking ac optimal power flow solutions. IEEE Transactions on Power Systems 2016;31(4):2809–23.
- [36] Qu G, Li N. Optimal distributed feedback voltage control under limited reactive power. IEEE Transactions on Power Systems 2020;35(1):315–31.
- [37] Magnsson S, Qu G, Li N. Distributed optimal voltage control with

- asynchronous and delayed communication. *IEEE Transactions on Smart Grid* 2020;11(4):3469–82.
- [38] Hirata K, Akutsu H, Ohori A, Hattori N, Ohta Y. Decentralized voltage regulation for pv generation plants using real-time pricing strategy. *IEEE Transactions on Industrial Electronics* 2017;64(6):5222–32.
- [39] Wang Y, Zhao T, Ju C, Xu Y, Wang P. Two-level distributed volt/var control using aggregated pv inverters in distribution networks. *IEEE Transactions on Power Delivery* 2020;35(4):1844–55.
- [40] Makhdoumi A, Ozdaglar A. Graph balancing for distributed subgradient methods over directed graphs. 2015. p. 1364–71.
- [41] Kekatos V, Zhang L, Giannakis GB, Baldick R. Voltage regulation algorithms for multiphase power distribution grids. *IEEE Transactions on Power Systems* 2016;31(5):3913–23.
- [42] Isham RBV. Non-negative matrices and markov chains. by e. seneta. *Journal of the Royal Statistical Society* 1983;146(2):202.
- [43] Su S, Lin Z. Distributed consensus control of multi-agent systems with higher order agent dynamics and dynamically changing directed interaction topologies. *IEEE Transactions on Automatic Control* Feb 2016;61(2):515–9.